Accepted Manuscript

Thermo-mechanical controls of flat subduction: Insights from numerical modeling

Pengpeng Huangfu, Yuejun Wang, Peter A. Cawood, Zhong-Hai Li, Weiming Fan, Taras V. Gerya

PII: S1342-937X(16)30232-5
DOI: doi: 10.1016/j.gr.2016.08.012
Reference: GR 1675

To appear in: *Gondwana Research*

Received date: 11 November 2015
Revised date: 9 August 2016
Accepted date: 17 August 2016

Please cite this article as: Huangfu, Pengpeng, Wang, Yuejun, Cawood, Peter A., Li, Zhong-Hai, Fan, Weiming, Gerya, Taras V., Thermo-mechanical controls of flat subduction: Insights from numerical modeling, *Gondwana Research* (2016), doi: 10.1016/j.gr.2016.08.012

Thermo-mechanical controls of flat subduction: insights from numerical modeling

Pengpeng Huangfu [1, 2], Yuejun Wang [1, 3, *], Peter A. Cawood [4, 5], Zhong-Hai Li [2], Weiming Fan [3], Taras V. Gerya [6]

1 School of Earth Science and Geological Engineering, Sun Yat-sen University, Guangzhou 510275, China
2 Key Laboratory of Computational Geodynamics, College of Earth Sciences, University of Chinese Academy of Sciences, Beijing 100049, China
3 CAS Center for Excellence in Tibetan Plateau Earth Sciences, Key Laboratory of Continental Collision and Plateau Uplift, Institute of Tibetan Plateau Research, Chinese Academy of Sciences, Beijing 100101, China
4 Department of Earth Sciences, University of St Andrews, North Street, St Andrews KY16 9AL, UK
5 Centre for Exploration Targeting, School of Earth and Environment, University of Western Australia, 35 Stirling Highway, Crawley, WA 6009, Australia
6 Institute of Geophysics, Department of Earth Sciences, ETH-Zurich, 8092 Zurich, Switzerland

Corresponding author current address:
School of Earth Science and Geological Engineering,
Sun Yat-sen University, Guangzhou 510275, China

Email: wangyuejun@mail.sysu.edu.cn

Abstract: Numerical experiments are used to investigate the thermo- mechanical controls for inducing flat subduction and why flat subduction is rare relative to normal/steep subduction. Our modeling results demonstrate that flat subduction is an end-member of a steady state subduction geometry and is characterized by a curved slab with a nearly-horizontal slab section. Intermediate cases between normal/steep and flat subduction appear to be transient in origin and evolve toward one of the stable end-members. Physical parameters inducing flat subduction can be classified into four categories: buoyancy of the subducting oceanic lithosphere (e.g., slab age, oceanic crustal thickness), viscous coupling between the overriding and downgoing plates (e.g., initial subduction angle), external kinematic conditions, and rheological properties of the subduction zone. On the basis of parameter sensitivity tests and the main characteristics of present-day flat subduction zones, positive buoyancy from either the young slab or the thickened oceanic crust are considered the primary controlling parameter. Our results show that the possibility of flat subduction is directly proportional to oceanic crustal thickness and inversely proportional to the slab age. Furthermore, oceanic crust must be thicker than 8 km to induce flat subduction, when the slab is older than 30 Ma with an initial subduction angle of $\geq 20°$, and without absolute trenchward motion of the overriding plate. The lower the initial subduction angle or the thicker the overriding continental lithosphere, the more likelihood for flat subduction. The initial subduction angle is more influential for the development of flat subduction than the overriding lithospheric thickness, and a thick overriding lithosphere induces flat subduction only under the condition of an initial

subduction angle of ≤ 25°, with a slab age of ≥ 30 Ma and without absolute trenchward motion of the overriding plate. However, when the initial subduction angle is increased to > 25°, no flat subduction is predicted. All the parameters are evaluated within the constraints of a mechanical framework in which the slab geometry is regarded as a result of a balance between the gravitational and hydrodynamic torque. Any factor that can sufficiently reduce gravitational torque or increase hydrodynamic torque will exert a strong effect on flat subduction development. Our results are consistent with the observations of modern flat subduction zones on Earth.

Keywords: flat subduction, numerical modeling, slab buoyancy, viscous interplate coupling, external kinematic conditions

1. Introduction

At convergent plate margins, variations in the dip of the downgoing slab of oceanic lithosphere in its upper 125 kilometers enable the division of subduction zones into low-angle (or flat) subduction (<30°), intermediate-angle subduction (between 30°-60°) and high-angle subduction (>60°) (e.g., Rodriguez-Gonzalez and Negredo, 2012). As shown in Fig. 1, flat subduction, which is characterized by a distinct flat-slab underlying the overriding lithosphere, occurs only in ~10 % of the world's convergent margins, e.g., Central Chile (Kay and Abbruzzi, 1996), Peru (Petford and Atherton, 1996), Ecuador (Beate et al., 2001), Costa Rica (Grafe et al., 2002; Gardner et al., 2013), SW Mexico (Suarez et al., 1990; Skinner and Clayton, 2011), Cascadia (Defant and Drummond, 1993), SE Alaska (Fuis et al., 2008) and Nankai Trough (Morris, 1995). Geological features ascribed to flat subduction include

compressive deformation and crustal-thickening in the overriding continental lithosphere, and a broad across-strike zone of arc magmatism with a magmatic gap and mineralization pulses (Gutscher et al., 2000a; Kay and Mpodozis, 2001; Sigloch et al., 2008). Flat subduction has been invoked to explain the geological characteristics in a number of ancient orogens, such as the end Mesozoic to early Paleogene orogenesis in western North America (e.g., Snyder et al., 1976; English et al., 2003) and the Mesozoic development of South China (e.g., Li and Li, 2007).

The causes of flat subduction remain debated, and a variety of explanations has been proposed, which can be grouped into the following six categories. (1) The most popular viewpoint is the buoyant nature of the downgoing oceanic slab due to either its overall young age or the thickened nature of the oceanic crust (Pilger, 1981; Brocher et al., 1994; Kay and Abbruzzi, 1996; Gutscher et al., 2000b; van Hunen et al., 2002b, 2004; Anderson et al., 2007; Espurt et al., 2008; Fuis et al., 2008; Sak et al., 2009; Skinner and Clayton, 2011). Both the young slab and the thickened oceanic crust can effectively reduce the average density of the oceanic slab, inhibiting the slab sinking steeply and promoting the development of low-angle subduction. (2) Thermal structure of the overriding continental lithosphere strongly correlates with the slab geometry (e.g., Rodriguez-Gonzalez et al., 2012). A colder overriding continental plate could induce a shallow slab to develop flat subduction, as a result of the increased viscosity of the mantle wedge and increased suction forces acting on the slab. (3) Trenchward motion of the overriding continental plate with respect to the downgoing slab exerts a significant influence on the slab dip angle (Uyeda and Kanamori, 1979; Jarrard, 1986; Lallemand et al., 2005). Vlaar (1983) proposed a "lithospheric doubling" scenario to relate the combined effects of active trenchward motion of the overriding continent and a relatively young oceanic lithosphere with the

development of flat subduction. (4) The slab dip angle might be influenced by rheological properties of the slab and surrounding mantle (van Hunen et al., 2001, 2002a, 2002b, 2004; Čížková et al., 2002; Billen and Hirth, 2005, 2007; Bellahsen et al., 2005; Manea and Gurnis, 2007). After the formation of flat subduction, a weak slab is favorable to resubduction from flat to steep subduction, whereas a highly strong slab will resist bending and descending (van Hunen et al., 2002b). A strong upper mantle might enhance flat subduction through increasing plate suction forces (van Hunen et al., 2004). (5) The interaction of the slab with large-scale mantle flow can greatly influence the slab dip angle (Ricard et al., 1991; Doglioni et al., 1999; Boutelier and Cruden, 2008). Physical modeling shows that overpressure on the slab lower surface induced by imposed mantle flow promotes shallow subduction but underpressure tends to induce steep subduction (Boutelier and Cruden, 2008). (6) Hydrodynamic forces (slab suction forces) are additionally proposed to account for flat subduction (Stevenson and Turner, 1977; Tovish et al., 1978). The low slab dip angle is attributed to strong slab suction. Other factors, which are believed to influence subduction pattern, include latent heat effects of the major mantle phase transitions, temperature of the basalt-to-eclogite transition, and viscosity of the mantle wedge (van Hunen et al., 2001, 2002a, 2002b; Skinner and Clayton, 2011).

Due to the limits of geological/geophysical observations in both time and depth, numerical modeling can play a significant role in developing and investigating geodynamic hypotheses, as well as better understanding plate tectonic process. Consequently, the synthesized approach integrating the field observations with geological, geochemical and geophysical data along with numerical modeling is widely applied in geosciences. Recently, topics concerning plate subduction/collision

dynamics have been systematically studied using numerical modeling, including: subduction initiation (e.g., Doin and Henry, 2001; Hall et al., 2003; Ueda et al., 2008; Nikolaeva et al., 2010; Cooper et al., 2011; Thielmann and Kaus, 2012; Marques et al., 2013; Leng and Guinis, 2015; Lu et al., 2015; Whattam and Stern, 2015); subduction processes (e.g., Sobolev and Babeyko, 2005; Billen and Hirth, 2007; Iwamori et al., 2007; Yamato et al., 2007; Babeyko and Sobolev, 2008; van Hunen and van den Berg, 2008; van Keken et al., 2008; Ribe, 2010; van Dinther et al., 2010; Angiboust et al., 2012; Li and Ribe, 2012; Baitsch-Ghirardello et al., 2014; Li et al., 2014; Vogt and Gerya, 2014;); and continental collision and orogen stabilization (e.g., Toussaint et al., 2004; Burov and Toussaint, 2007; Göğüş and Pysklywec, 2008; Yamato et al., 2008; Faccenda et al., 2009; Li et al., 2011; Burov et al., 2012; Gray and Pysklywec, 2012; Gorczyk et al., 2013; Replumaz et al., 2014; Sizova et al., 2014).

In this paper, parameter sensitivity analysis has been performed using numerical modeling in order to investigate how the subduction pattern is correlated with the main geodynamic parameters of oceanic lithospheric age, oceanic crustal thickness, initial subduction angle, thermal structure of the overriding continental plate, external kinematic conditions, and rheological properties of the continental lithosphere and asthenospheric mantle. In addition, we outline conditions under which flat subduction is possible and under which it is impossible, and discuss these results with respect to the main geodynamic features at modern flat subduction zones. Finally, all the parameters are re-evaluated in a mechanical framework.

2. Numerical model description

The numerical models are constructed with the thermo-mechanical code "I2VIS" (Gerya and Yuen, 2003, 2007) based on the finite difference method and maker-in-cell techniques. Details of the numerical methodology are shown in Supplementary Material 1. All abbreviations and units used are listed in Supplementary Dataset Table 1. Large-scale numerical models (4000×670 km, Fig. 2) were constructed to evaluate variables that may lead to flat subduction. The models consist of a non-uniform 699×134 rectangular grid with a resolution varying from 2×2 km in the vicinity of the subduction zone to 30×30 km further away. The lithological structure of the model is represented by a dense grid of ~7 million active Lagrangian markers for advecting various material properties and temperatures. The rheology of rocks is composition-, pressure-, temperature-, and strain rate-dependent and accounts for brittle and ductile deformation of crustal and mantle rocks, respectively. Detailed properties of different rock types are shown in Supplementary Dataset Tables 2-3.

The numerical models incorporate an oceanic domain on the left and a continental domain on the right. The oceanic domain comprises oceanic crust, oceanic lithospheric mantle, and underlying asthenospheric mantle, and all three layers have variable thicknesses depending on the models being evaluated (Table 1). The continental domain consists of a sedimentary layer (6 km thick), upper crust (14 km thick), lower crust (15 km thick), lithospheric mantle and asthenosphere with variable thickness depending on the evaluated models (Table 1).

The boundary conditions used in the models are free slip at all boundaries except the lower boundary, which is treated as being permeable to satisfy free slip at an external boundary at 1000 km below the base of the model (Burg and Gerya, 2005;

Ueda et al., 2008; Li et al., 2010). External free slip must conform to global conservation of mass in the computational domain and is implemented by using the following limitation for velocity components at the lower boundary: $\partial v_x/\partial z = 0$, $\partial v_z/\partial z = -v_z/\Delta z_{external}$, where $\Delta z_{external}$ is the vertical distance from the lower boundary to the external boundary where free slip ($\partial v_x/\partial z = 0, v_z = 0$) is satisfied. The pushing and overthrusting velocities, which refer to the absolute subduction velocity of the downgoing slab and the absolute trenchward velocity of the overriding continental lithosphere, respectively, are assigned to a small internal domain within the oceanic and continental lithospheres, respectively, but the values are dependent on the evaluated models (Table 1). It is worth noting that, within the globally 3-D confined system of plates, 'external push' imposed on a plate (and coming from different neighboring slabs) can be significant. In the numerical models, we use prescribed convergence velocity condition as an approximation of external push, which is much easier for implementation and better for understanding. Besides the prescribed external push, growing slab pull is naturally present in the numerical models due to the differences in temperature (and density) between subducting slab and surrounding mantle. Slab pull results in spontaneous slab bending and subduction of the downgoing slab. Variable boundary conditions including external push versus slab pull are studied in Li and Gerya (2009). Such boundary conditions are a reasonable approximation of nature, and thus can be applied in many numerical simulations of subduction and collision processes (e.g., Gerya, 2011; Li, 2014). In addition, although 2D and 3D models have several differences, especially concerning

the transverse deformation and quasi-toroidal mantle flow around the slab edges, they share a number of dynamic similarities including slab bending mechanics and subduction mode selection (Ribe, 2010; Li and Ribe, 2012). As a result, the 2D model is appropriate for studying the first-order mechanism of flat subduction.

The initial thermal structure of oceanic lithosphere is simplified to be linearly interpolated with 0 °C at the surface and 1300 °C at the base of the lithospheric mantle. However, the thickness of oceanic lithosphere depends on its age (Turcotte and Schubert, 2002). The initial thermal structure of continental lithosphere is laterally uniform with 0 °C at the surface and 1300 °C at the base of the continental lithospheric mantle (Turcotte and Schubert, 2002). The initial temperature gradient in the asthenospheric mantle is 0.5 °C/km. The thermal boundary conditions have fixed values for the upper boundary (0 °C at the surface) and zero horizontal heat flux across the vertical boundaries. For the lower thermal boundary, an infinity-like external constant temperature condition is imposed (Burg and Gerya, 2005; Ueda et al., 2008; Li et al., 2010), which allows both temperature and vertical heat flux to vary along the permeable box lower boundary, ensuring that the constant temperature condition is satisfied at around 1000 km below the base of the model. This condition is implemented by using the equation $\partial T/\partial z = (T_{external} - T)/\Delta z_{external}$, where $T_{external}$ is the temperature at the external boundary and $\Delta z_{external}$ is the vertical distance from the lower boundary to the external boundary.

3. Numerical modeling results

The model results (Figs. 3-8) demonstrate that flat subduction is a distinct end-member of steady-state subduction geometry characterized by a strongly curved slab with an obvious nearly-horizontal section. Intermediate cases between normal/steep and flat subduction appear to be transient and evolve towards one of the stable (normal/steep or flat) end-members. Parameters related to the development of flat subduction include slab age, oceanic crustal thickness, the initial subduction angle, thermal structure of the overriding continental lithosphere, absolute trenchward velocity of the overriding continent, rheological properties of the overriding continental crust and the asthenosphere. The effects of these parameters can be grouped into four types, with changing (1) the slab buoyancy, (2) viscous interplate coupling between the subducting and the overriding plate, (3) external kinematic conditions, and (4) rheological properties of the subduction zone. Figures 3-8 show the numerical results for evaluating the effects of variable parameters on the formation of flat subduction.

3.1. Slab buoyancy

Thickened oceanic crust or a buoyant slab (e.g., aseismic ridges, bathymetric highs, and oceanic plateaus) have been proposed as key factors for inducing flat subduction, since positive buoyancy can inhibit the slab sinking steeply (e.g., Gutscher et al., 2000a; van Hunen et al., 2000, 2002a, 2002b; Gutscher, 2002; Perez-Gussinye et al., 2008). Slab age and oceanic crustal thickness are two principle parameters to determine the slab buoyancy.

Slab age: Thickness of oceanic lithosphere is proportional to its age (Parsons and Sclater, 1977), reflecting its increasing density. The average density of young oceanic lithosphere is generally low (Cloos, 1993). Therefore, a young oceanic slab is more willing to induce flat subduction than an old slab. The numerical results for models M1-1~M1-6 (Table 1) show that, under a low initial subduction angle of 15º, flat subduction can be developed, even when the slab age is increased to 60 Ma. However, at an initial subduction angle of 20º (models M1-7~M1-12, Fig. 3), flat subduction is replaced by steep subduction, when the slab age increases from 30 Ma to 40 Ma, due to the corresponding increase in the slab negative buoyancy .

Oceanic crustal thickness: Models M2-1 to M2-11 systematically explore how the thickened oceanic crust influences the subduction pattern, and how the thickness of the oceanic crust and the age of oceanic lithosphere jointly regulate the formation of flat subduction. For oceanic lithosphere with an age of 40 Ma (M2-1, Table 1), flat subduction occurs when oceanic crustal thickness is greater than 11 km. As the age of the downgoing slab increases, the threshold value of oceanic crustal thickness for inducing flat subduction is also increased, because larger positive buoyancy from the subducted oceanic crust is required to balance the increasing negative buoyancy from the older and thickened oceanic lithosphere. For example, for 50 Ma oceanic lithosphere (M2-2 and M2-3), an oceanic crustal thickness of 17 km is required to induce flat subduction; for 60 Ma oceanic lithosphere (M2-4 and M2-5), the thickness needs to be greater than 20 km. Further simulations (M2-6 and M2-7, Fig. 4) reveal that the threshold value of the oceanic crustal thickness for inducing flat subduction

rises to greater than 29 km for 80 Ma oceanic lithosphere (Fig. 4b). Additionally, numerical results of M1-9, M2-8 and M2-9 with an identical slab age (Table 1) show that an increase in initial subduction angle greatly counteracts the effect of increasing oceanic crustal thickness on the development of flat subduction. Specifically, for a slab age of 30 Ma, flat subduction occurs with an initial subduction angle of 20°, even when the oceanic crustal thickness is only 8 km. However, when the initial subduction angle increases to 30º, flat subduction occurs only when the oceanic crustal thickness is greater than 17 km. Comparison of results of model M2-1 with M2-10 and M2-11 demonstrates a similar tendency.

3.2. Viscous interplate coupling

Interplate coupling refers to the ability to lock and accumulate stress between two plates. Strong interplate coupling can prevent detachment of the subducting slab from the overriding plate, and thus facilitate the formation of flat subduction. The degree of interplate coupling is mainly affected by the size of the contact area and the viscosity of the interface (or interlayer) between the slab and overriding plate.

Initial subduction angle: The initial subduction angle directly determines the contact area of the adjacent plates for interplate coupling. Numerical results, as shown in Fig. 5, demonstrate that subduction pattern changes from normal/steep subduction to flat subduction with a reduction in the initial subduction angle. The results (Table 1 and Fig. 5) illustrate subduction patterns under the conditions of the oceanic slab with an age of 40 Ma and various initial subduction angles, indicating that the models with

an initial dip of 20º or greater are characterized by steep subduction, but those with an initial angle of 15º or lower experience flat subduction. A similar tendency of the subduction pattern is revealed for models with 20 Ma (M1-14, M1-8 and M1-2, Table 1) and 30 Ma oceanic lithosphere (M1-15, M1-9 and M1-3, Table 1). Generally, a low initial subduction angle indicates strong interplate viscous coupling, which in turn leads to a high degree of upper plate seismicity, intense upper plate deformation, strong stress field, and cold thermal structure. Thus, our results show that the lower the initial subduction angle, the stronger the interplate coupling, and the greater chance for flat subduction.

Thermal structure of the overriding continental lithosphere: Development of the flat subduction is strongly controlled by the mechanical behavior of oceanic and continental lithosphere, which is highly dependent on temperature (McKenzie et al., 2005). A series of numerical models were designed to investigate how the thermal structure of the overriding continental lithosphere influences the formation of flat subduction (M1-10, M4-1 and M4-2, Table 1). The numerical results of these models show the colder the overriding continental lithosphere, the more likely it is to induce flat subduction. Flat subduction occurs when the thickness of the continental lithosphere (i.e., the depth of 1300 °C isotherm) is greater than 130 km (Fig. 6b), under conditions of a 40 Ma-old oceanic slab and an initial subduction angle of 20º. The effect of thermal structure of the overriding plate on slab dip angle is related to the suction force (interplate coupling) in the mantle wedge (Rodriguez-Gonzalez and Negredo, 2012). Viscosity at the base of a cold overriding plate is higher than that of a

hot overriding plate, generating a relatively greater hydrodynamic suction force (stronger interplate coupling). Thus, low-angle subduction can be predicted, when the oceanic plate sinks underneath a cold continental lithosphere.

3.3. External kinematic conditions

A series of numerical models (M3-1~M3-6, Table 1) were designed to investigate the effect of the trenchward motion of the overriding continental plate with respect to the downgoing slab on the development of flat subduction. For models with a low absolute subduction velocity (< 2.5 cm/a) of the downgoing slab, a low absolute trenchward velocity (~1 cm/a) of the overriding lithosphere can induce flat subduction. However, for the models with an absolute subduction velocity of 5 cm/a for the downgoing slab, an overthrusting velocity of 5 cm/a or greater for the overriding continental plate is required to induce flat subduction (M3-6; Fig. 7). Two main reasons have been proposed for such numerical results: (1) given the same interplate coupling, a high absolute subduction velocity promotes the detachment of the underlying slab from the overriding plate, and (2) a high absolute trenchward velocity of the overriding plate facilitates slab upward bending to transform subduction pattern from normal to low-angle subduction. The higher the overthrusting velocity, the easier it is to achieve the transformation to flat subduction.

3.4. Rheological properties of the subduction zone

In this section, we study the effects of rheological properties of the continental

crust and the asthenosphere on the subduction patterns.

Rheological property of the continental crust: The rheological strength of the continental crust can influence the development of flat subduction. When the continental crust is weak, it is easy for the converging oceanic plate to deform the overriding continental crust, which favors a steep subduction pattern. On the contrary, if the continental crust is strong, then deformation of the overriding continental crust is limited, and the subduction angle most likely maintains its initial state. Therefore, under the same initial settings and boundary conditions, models with strong overriding continental crust would result in flat subduction. Specifically, for model M5-1 (Fig. 8a), it is observed that weak overriding continental crust accompanying strong deformation results in steepening of the subducting slab. However, the result of model M5-2 (Fig. 8b), for which the initial continental crustal viscosity is 5 times higher than that of model M5-1, shows that the subduction angle largely remains unchanged, and flat subduction develops. Similar numerical result is obtained for the model with an initial continental crustal viscosity being up to 10 times of model M5-1, as shown in Fig. 8c.

Rheological property of the asthenosphere: Three numerical models (M1-10, M6-1 and M6-2) are designed for evaluating the effect of the rheological properties of the asthenosphere on subduction patterns. Our numerical results show that models with weak asthenosphere are more likely to develop flat subduction than those with strong asthenosphere. Specifically, model M1-10 demonstrates that flat subduction cannot develop where a strong asthenosphere inhibits bending of the subducted slab

(Fig. 8d). When the asthenospheric viscosity is weakened by 10 times relative to that of M1-10, as shown in model M6-1, a similar result is given (Fig. 8e). However, when the value of asthenospheric viscosity is 100 times lower than that of M1-10, as shown in M6-2 (Fig. 8f), flat subduction develops due to the decreasing of resistance force from the asthenosphere during the slab upward bending process. Thus, although asthenospheric rheology is less sensitive in its ability to regulate the subduction pattern, it might still have a limiting effect on the development of flat subduction under the favorable mechanical and thermal conditions.

4. Discussion

4.1. What are the favorable conditions for flat subduction?

Our numerical experiments indicate that the development of flat subduction can be attributed to positive buoyancy of the downgoing plate, strong plate coupling along the subduction interface, favorable external kinematic conditions, and beneficial rheological properties of the subduction zone. However, rheological properties appear to be the least significant given the generally low variability of rheological properties in the vicinity of subduction zones. The other three principal types of parameters can separately or jointly induce flat subduction.

The presence of either thickened oceanic crust or young oceanic lithosphere usually reflects positive buoyancy of the downgoing slab. The positive buoyancy can inhibit the slab subducting steeply, which is favourable to transforming the subduction pattern from normal to flat subduction. Generally, young oceanic slab is warmer,

thinner, and more buoyant than the older slab, resulting in a decrease in the average density, thus enhancing the possibility of flat subduction. The results of models with variable slab age and oceanic crustal thickness are shown in Fig. 9a. These results demonstrate that the possibility of flat subduction is directly proportional to oceanic crustal thickness and inversely proportional to slab age, when the other parameters are constant. Our results also indicate that, to induce flat subduction, the oceanic crust must be thicker than the average oceanic crustal thickness (8 km), when the slab age is older than 30 Ma (Fig. 9a). Such a numerical result is consistent with the observation that the subducting plates in regions experiencing flat subduction on the present-day Earth are always younger than 50 Ma, with the majority being younger than 30 Ma. Figure 9a also shows that, to induce flat subduction where the age of the oceanic slab is older than 60 Ma, the thickness of oceanic crust must be greater than 20 km. Such a great thickness of oceanic crust is rarely observed. This explains the poor development of flat subduction in the West Pacific, Indian, and Atlantic oceans, where the subducted slab is generally older than 60 Ma.

Strong viscous interplate coupling along the subduction interface can prevent detachment of the oceanic slab from the overriding continental plate. Strong coupling is usually obtained through increasing the contact area between the plates or increasing viscosity of the subduction channel. Additional numerical experiments are designed to systematically investigate the relationship of the combined effects of the initial subduction angle and overriding continental lithospheric thickness with the subduction pattern. Numerical results in Figs. 9b-c indicate that the thicker the

overriding continental lithosphere or the lower the initial subduction angle, the greater likelihood of flat subduction. Furthermore, the initial subduction angle seems to be more significant for the flat subduction development, compared with the thickness of overriding continental lithosphere. After the initial subduction angle rises to greater than 25°, flat subduction cannot occur, even if the overriding continental lithospheric thickness reaches 240 km. The comparative modeling in Figs. 9b-c also suggests that, for an older oceanic slab with relatively greater negative buoyancy, a thicker overriding continental lithosphere is required to induce flat subduction under the same initial subduction angle (less than 25°). It is worth noting that although strong plate coupling indicates a high possibility of flat subduction, at the same time, increasing plate coupling along the lengthened subduction channel after the formation of flat subduction will also affect the plate dynamic processes, such as decreasing the convergence rate or affecting the orogenic process (Martinod et al., 2010).

Favorable external kinematic conditions (i.e., the absolute trenchward motion of the overriding plate) can cause mechanical bending of the subducting slab, transforming normal subduction into flat subduction. In Fig. 7, trenchward motion of the overriding plate leads to upward bending of the slab. Additional numerical results (Fig. 9d) show that, given a slab age of 40 Ma, a low absolute trenchward velocity (~ 1 cm/a) of the overriding continental lithosphere can induce flat subduction, when the absolute subduction velocity of the oceanic slab is less than 3 cm/a. However, under the condition of the absolute subduction velocity of > 3 cm/a, flat subduction occurs only when the absolute trenchward velocity is not less than the absolute subduction

velocity. This result is also consistent with the geological observations for present-day flat subduction zones on Earth, in which the overriding continental lithosphere commonly has a high absolute trenchward velocity (Fig. 1). In general, all external kinematic conditions beneficial to the horizontal flexure of the subducting slab promote the formation of flat subduction.

4.2. Why is flat subduction rare relative to normal/steep subduction?

Available data show that flat subduction only occurs in around 10 % of global subduction zones (e.g., Gutscher et al., 2000a; Gutscher et al., 2000b; van Hunen et al., 2002b; Skinner and Clayton, 2011). The main geodynamic parameters for regions of flat subduction are summarized in Fig. 1 (e.g., Central Chile, Peru, Ecuador, Costa Rica, Southwestern Mexico, Cascadia, Southeastern Alaska, and Southwestern Japan).

Our numerical experiments demonstrate that a combination of "abnormal" mechanical and thermal conditions needs to be satisfied to induce flat subduction. For example, when the oceanic slab is older than 30 Ma at the initial subduction angle of 20°, a thickened oceanic crust (> 8 km) is required for flat subduction. Furthermore, for the slab older than 30 Ma, each 10 Ma increase in slab age will require an additional oceanic crustal thickness of ~3 km to balance the increasing negative buoyancy of the slab, as shown in Fig. 9a. Under the conditions of a 60 Ma-old oceanic slab with an average crustal thickness (6-8 km) and an initial subduction angle of 25°, an overriding continental lithosphere thicker than 200 km is needed to enable the formation of flat subduction (Fig. 9c). For a 40 Ma-old oceanic slab and an

absolute subduction velocity of larger than 3.5 cm/a, the absolute trenchward velocity of the overriding continental lithosphere should be not less than the absolute subduction velocity of the oceanic slab to induce flat subduction (Fig. 9d).

Most examples of flat subduction on Earth share three thermo-mechanical features, involving buoyancy anomaly of the oceanic slab, absolute trenchward motion of the overriding continental plate, and thickened overriding continental lithosphere (Fig. 1). Available data show that the oceanic slab in the present-day flat subduction zone is always younger than 50 Ma with the majority of ≤ 30 Ma (with exception of Central Chile, Peru, and Cascadia), which is younger than the average age of oceanic crust of 60 Ma (Condie, 1997). However, subduction of a spreading ridge inhibits flat subduction in contrast to adjoining regions of young buoyant oceanic crust. This might reflect that the formation of a slab window, with quasi-toroidal mantle flow around the slab edge (e.g., Espurt et al., 2007; Groome and Thorkelson, 2009). Most examples of flat subduction show that the absolute trenchward velocity of the overriding continental lithosphere is greater than the absolute subduction velocity of the downgoing plate (Fig. 1). The thickened overriding continental lithosphere is observed in most examples of the present-day flat subduction. For flat subduction in Peru and Central Chile, thickness of the overriding continental lithosphere ranges from 140 km to 200 km. However, for the steep subduction in the Altiplano located between these two flat subduction zones, the thickness only reaches 100 ± 25 km (Perez-Gussinye et al., 2008). The variety of the subduction angle of the Cocos slab beneath Central America is also considered to be related to the overriding lithospheric

thickness. Flat subduction beneath the Maya Block of SW Mexico possesses a cold overriding continental lithosphere, but steep subduction beneath Chortis Block of Caribbean plate corresponds to a relatively warmer upper plate (Rodriguez-Gonzalez and Negredo, 2012).

On the basis of the numerical results and the principal features of present-day flat subduction zones (Fig. 1), it is proposed that the positive buoyancy resulting from the subduction of either a young slab or thickened oceanic crust should be the primary controlling parameter on the development of flat subduction. Nevertheless, other parameters, for example viscous interplate coupling, external kinematic conditions and rheological properties of the subduction zone, can also affect the formation of flat subduction.

4.3 Evaluation of the parameters in a mechanical framework

Despite the fact that a variety of factors affect slab dip, the first order control on slab dynamics can be attributed to a balance of driving forces and resisting forces (Stevenson and Turner, 1977; Manea et al., 2006). The driving forces are regarded as the resultant force induced by the combined effects of slab gravity and slab buoyancy, which can be quantitatively defined as gravitational torque per unit slab width t_G (Rodriguez-Gonzalez et al., 2012):

$$t_G = \frac{T_G}{D} = \int_0^l \Delta\rho(\alpha, r) ghr \cos a dr \quad (1)$$

where D is the slab width, $\Delta\rho$ is the density contrast between the slab and the surrounding mantle material, l is the slab length, h is the slab thickness, r is the

radial coordinate with the origin placed at the base of the lithosphere in the plate boundary, and α is the slab dip angle. This torque reflects the magnitude of the downward-sinking tendency of the slab. A young oceanic slab or a thickened oceanic crust commonly causes a decrease in gravitational torque, inhibiting the slab sinking steeply and promoting the development of low-angel subduction. The resisting forces are mainly induced by rheological effects and can be described as the hydrodynamic torque (suction torque) per unit slab width t_H (Rodriguez-Gonzalez et al., 2012), which exerts a suction force on the slab:

$$t_H = \frac{T_H}{D} = \int_0^l [P_A(\alpha, r) - P_B(\alpha, r)] r dr \quad (2)$$

where P_A and P_B are the pressures acting on the slab upper and lower surfaces, respectively. Both pressures may be varied by the shear stresses of the mantle flow, which are strongly correlated to the viscosity of the surrounding mantle and relative velocity of the slab with the surrounding mantle (McKenzie, 1969). Since both pressures act in the upward direction, the pressure difference and the hydrodynamic torque across the slab always work to reduce the slab dip angle (Stevenson and Turner, 1977).

In this mechanical framework, slab geometry is strongly correlated with the balance of the gravitational and hydrodynamic torque. The former tends to cause the slab to subduct deeply and steeply, but the latter contributes to decreasing the subduction angle. Thus, low-angle subduction or flat subduction can be expected under conditions that can sufficiently reduce the gravitational torque or increase the hydrodynamic torque. In contrast, steep subduction is usually associated with a higher

gravitational torque or a lower hydrodynamic torque.

Using this mechanical framework, it is believed that the qualitative mechanical analysis can reasonably account for the above numerical results and enhance our understanding of the fundamental reason for flat subduction. However, the quantification of gravitational torque and suction torque in the current numerical models are difficult. Thus we focus on the qualitative mechanical analysis in this study. Almost all the parameters influence slab dip angle through changing the gravitational torque or suction torque. For example, a young oceanic slab or thickened oceanic crust can effectively decrease the gravitational torque, causing the slab to move upward with a decreasing dip angle. A low initial subduction angle, a thick overriding continental plate, or high rheological strength of the continental crust can increase the suction torque by increasing the pressure on the slab upper surface, i.e. P_A in equation (2), to finally reduce the slab dip angle.

Flat subduction caused by increasing the absolute trenchward velocity of the overriding continental plate is ascribed to the combined effects of an increase in the pressures beneath and above the slab, as shown in Figs. 10a-b. The former results from a rise in the relative velocity between the slab and overriding plate, whereas the latter is dominated by the induced landward mantle flow beneath the slab with increasing intensity (Fig. 10b). Both can effectively increase the suction torque of the slab, consequently leading to flat subduction. Such an explanation for flat subduction induced by the trenchward motion of the overriding plate appears more reasonable than the “lithospheric doubling” scenario (Vlaar, 1983), in which both the trenchward

motion of the overriding plate and subduction of relatively young oceanic lithosphere inhibit the slab sinking to cause the development of flat subduction.

The numerical results show that weak asthenospheric mantle promotes the development of flat subduction, which at first seems paradoxical. Decreasing the asthenospheric viscosity, on one hand, leads to a decrease in hydrodynamic torque. However, on the other hand, decreasing the asthenospheric viscosity also decreases the resistance forces acting on the slab upper surface by the mantle wedge in the creation of a flat slab. The two effects counteract each other. The former favors steep subduction, but the latter promotes flat subduction. Our numerical results indicate that the second effect prevails over the first one, i.e., decreasing the mantle viscosity will reduce the resistance forces acting on the slab upper surface during slab upward bending process, thus allowing the necessary mantle wedge deformation for the slab flattening and enhancing the development of flat subduction. In this aspect, our results are consistent with that of van Hunen et al. (2002), in which the model without a weakened mantle wedge does not show any development of a flat-slab segment, whereas the model with one order of magnitude weakening of mantle wedge develops flat subduction.

Based on the above analyses, it is believed that the slab geometry can be regarded as a result of a balance of the gravitational torque and the hydrodynamic torque of the slab. Almost all the tested parameters can be incorporated into this mechanical framework to further account for the slab dip variability by changing either the gravitational torque or the suction torque, except the rheological property of

asthenospheric mantle, for which the effects on deformation behaviour of the overriding mantle wedge should be taken into account at the same time. In addition, the sensitivity test of the subduction pattern to the crustal rheological strength of the overriding plate, which has been rarely discussed, reveals that the deformation behavior of the overriding plate in the subduction zone can also affect the slab geometry.

5. Conclusions

Our thermo-mechanical experiments demonstrate that flat subduction is an important end-member of the geometry of a subduction zone and is characterized by a curved slab with a large near-horizontal slab section. Intermediate cases between normal/steep and flat subduction seem to be transient and evolve toward one of the stable (normal/steep or flat) end-members. Parameters, which control the formation of flat subduction, can be classified into four main categories involving buoyancy of the subducting oceanic slab (e.g., the slab age, oceanic crustal thickness), viscous interplate coupling of the overriding with downgoing plate (e.g., the initial subduction angle, thermal structure of the overriding lithosphere), external kinematic conditions (e.g., absolute trenchward motion of the overriding plate), and rheological properties of the subduction zone (e.g., rheological properties of the overriding continental crust and the asthenospheric mantle). Correspondingly, our numerical experiments indicate that the development of flat subduction can be attributed to four types of conditions involving positive buoyancy of the downgoing plate, strong plate coupling along the

subduction interface, favorable external kinematic conditions, and beneficial rheological properties of the subduction zone. On the basis of parameter sensitivity tests and data from zones of present-day flat subduction, it is believed that positive buoyancy, from either the thickened oceanic crust or the young slab, is the primary controlling parameter, although the other parameters can also affect slab dip angle. In most cases, these parameters jointly control and regulate the subduction pattern.

In order to investigate the fundamental reasons for slab dip variability, almost all the tested parameters were further evaluated in a mechanical framework, where slab dynamics is attributed to the balance of the gravitational torque and the hydrodynamic torque (suction torque). We find that any factor that can sufficiently reduce the gravitational torque or increase the hydrodynamic torque will exert a highly positive effect on the development of flat subduction. Almost all the tested parameters can be incorporated into the mechanical framework to account for the various subduction patterns through changing the gravitational torque or the hydrodynamic torque.

Acknowledgements

We would like to thank the editor Prof. Nick Rawlinson and two anonymous reviewers for their critical and constructive reviews on this paper. This study was supported by National Basic Research Program of China (2014CB440901), the Strategic Priority Research Program (B) of CAS (XDB18020104), National Science Foundation of China (41190073, 41372198 and 41304071), and NERC grant NE/J021822/1.

References

Anderson, M., Alvarado, P., Zandt, G., Beck, S., 2007. Geometry and brittle deformation of the subducting Nazca Plate, Central Chile and Argentina. Geophysical Journal International 171, 419-434.

Angiboust, S., Wolf, S., Burov, E., Agard, P., Yamato, P., 2012. Effect of fluid circulation on subduction interface tectonic processes: Insights from thermo-mechanical numerical modelling. Earth and Planetary Science Letters 357-358, 238-248.

Babeyko, A.Y., Sobolev, S.V., 2008. High-resolution numerical modeling of stress distribution in visco-elasto-plastic subducting slabs. Lithos 103, 205-216.

Baitsch-Ghirardello, B., Gerya, T.V., Burg, J.-P., 2014. Geodynamic regimes of intra-oceanic subduction: Implications for arc extension vs. shortening processes. Gondwana Research 25, 546-560.

Ballmer, M.D., Ito, G., Wolfe, C.J., Solomon, S.C., 2013. Double layering of a thermochemical plume in the upper mantle beneath Hawaii. Earth and Planetary Science Letters 376, 155-164.

Bellahsen, N., Faccenna, C., Funiciello, F., 2005. Dynamics of subduction and plate motion in laboratory experiments: Insights into the "plate tectonics" behavior of the Earth. Journal of Geophysical Research-Solid Earth 110.

Beate, B., Monzier, M., Spikings, R., Cotten, J., Silva, J., Bourdon, E., Eissen, J.P., 2001. Mio-Pliocene adakite generation related to flat subduction in southern Ecuador: the Quimsacocha volcanic center. Earth and Planetary Science Letters 192, 561-570.

Billen, M.I., Hirth, G., 2005. Newtonian versus non‐Newtonian upper mantle viscosity: Implications for subduction initiation. Geophysical Research Letters 32.

Billen, M.I., Hirth, G., 2007. Rheologic controls on slab dynamics. Geochemistry, Geophysics, Geosystems 8, Q08012.

Bossmann, A.B., van Keken, P.E., 2013. Dynamics of plumes in a compressible mantle with phase changes: Implications for phase boundary topography. Physics of the Earth and Planetary Interiors 224, 21-31.

Boutelier, D.A., Cruden, A.R., 2008. Impact of regional mantle flow on subducting plate geometry and interplate stress: insights from physical modelling. Geophysical Journal International 174, 719-732.

Brocher, T.M., Fuis, G.S., Fisher, M.A., Plafker, G., Moses, M.J., Taber, J.J., Christensen, N.I., 1994. Mapping the Megathrust beneath the Northern Gulf of Alaska Using Wide-Angle Seismic Data. Journal of Geophysical Research-Solid Earth 99, 11663-11685.

Burg, J.P., Gerya, T., 2005. The role of viscous heating in Barrovian metamorphism of collisional orogens: thermomechanical models and application to the Lepontine Dome in the Central Alps. Journal of Metamorphic Geology 23, 75-95.

Burov, E., Francois, T., Yamato, P., Wolf, S., 2012. Mechanisms of continental subduction and exhumation of HP and UHP rocks. Gondwana Research.

Burov, E., Toussaint, G., 2007. Surface processes and tectonics: forcing of continental subduction and deep processes. Global and Planetary Change 58, 141-164.

Condie, K.C., 1997. Plate Tectonics. Butterworth-Heinemann.

Cooper, F.J., Platt, J.P., Anczkiewicz, R., 2011. Constraints on early Franciscan subduction rates from 2-D thermal modeling. Earth and Planetary Science Letters 312, 69-79.

Cloos, M., 1993. Lithospheric buoyancy and collisional orogenesis: Subduction of oceanic plateaus, continental margins, island arcs, spreading ridges, and seamounts. Geological Society of America Bulletin 105: 715-737.

Davies, D.R., Davies, J.H., 2009. Thermally-driven mantle plumes reconcile multiple hot-spot observations. Earth and Planetary Science Letters 278, 50-54.

Defant, M.J., Drummond, M.S., 1993. Mount-St-Helens - Potential Example of the Partial Melting of the Subducted Lithosphere in a Volcanic Arc. Geology 21, 547-550.

Doglioni, C., Harabaglia, P., Merlini, S., Mongelli, F., Peccerillo, A., Piromallo, C., 1999. Orogens and slabs vs. their direction of subduction. Earth-Science Reviews 45, 167-208.

Doin, M.P., Henry, P., 2001. Subduction initiation and continental crust recycling: the roles of rheology and eclogitization. Tectonophysics 342, 163-191.

Dymkova, D., Gerya, T., Burg, J.-P., 2D thermomechanical modelling of continent–arc–continent collision. Gondwana Research.

English, J.M., Johnston, S.T., Wang, K., 2003. Thermal modelling of the Laramide orogeny: testing the flat-slab subduction hypothesis. Earth and Planetary Science Letters 214, 619-632.

Espurt, N., Baby, P., Brusset, S., Roddaz, M., Hermoza, W., Regard, V., Antoine, P.O., Salas-Gismondi, R., Bolanos, R., 2007. How does the Nazca Ridge subduction influence the modern Amazonian foreland basin? Geology 35, 515-518.

Espurt, N., Funiciello, F., Martinod, J., Guillaume, B., Regard, V., Faccenna, C., Brusset, S., 2008. Flat subduction dynamics and deformation of the South American plate: Insights from analog modeling. Tectonics 27.

Faccenda, M., Minelli, G., Gerya, T., 2009. Coupled and decoupled regimes of continental collision: numerical modeling. Earth and Planetary Science Letters 278, 337-349.

Farnetani, C.G., Hofmann, A.W., 2009. Dynamics and internal structure of a lower mantle plume conduit. Earth and Planetary Science Letters 282, 314-322.

Fuis, G.S., Moore, T.E., Plafker, G., Brocher, T.M., Fisher, M.A., Mooney, W.D., Nokleberg, W.J., Page, R.A., Beaudoin, B.C., Christensen, N.I., Levander, A.R., Lutter, W.J., Saltus, R.W., Ruppert, N.A., 2008. Trans-Alaska Crustal Transect and continental evolution involving subduction underplating and synchronous foreland thrusting. Geology 36, 267-270.

Gardner, T.W., Fisher, D.M., Morell, K.D., Cupper, M.L., 2013. Upper-plate deformation in response to flat slab subduction inboard of the aseismic Cocos Ridge, Osa Peninsula, Costa Rica. Lithosphere 5, 247-264.

Gerya T V. 2011. Future directions in subduction modeling. J Geodynamics, 52: 344-378

Gerya, T.V., Yuen, D.A., 2003. Characteristics-based marker-in-cell method with

conservative finite-differences schemes for modeling geological flows with strongly variable transport properties. Physics of the Earth and Planetary Interiors 140, 293-318.

Gerya, T.V., Yuen, D.A., 2007. Robust characteristics method for modelling multiphase visco-elasto-plastic thermo-mechanical problems. Physics of the Earth and Planetary Interiors 163, 83-105.

Glišović, P., Forte, A.M., 2014. Reconstructing the Cenozoic evolution of the mantle: Implications for mantle plume dynamics under the Pacific and Indian plates. Earth and Planetary Science Letters 390, 146-156.

Göğüş, O.H., Pysklywec, R.N., 2008. Near-surface diagnostics of dripping or delaminating lithosphere. Journal of Geophysical Research: Solid Earth (1978–2012) 113.

Gonzalez, C.M., Gorczyk, W., Gerya, T.V., Decarbonation of subducting slabs: Insight from petrological–thermomechanical modeling. Gondwana Research.

Gorczyk, W., Hobbs, B., Gessner, K., Gerya, T., 2013. Intracratonic geodynamics. Gondwana Research 24, 838-848.

Grafe, K., Frisch, W., Villa, I.M., Meschede, M., 2002. Geodynamic evolution of southern Costa Rica related to low-angle subduction of the Cocos Ridge: constraints from thermochronology. Tectonophysics 348, 187-204.

Gray, R., Pysklywec, R.N., 2012. Geodynamic models of mature continental collision: Evolution of an orogen from lithospheric subduction to continental retreat/delamination. Journal of Geophysical Research: Solid Earth (1978–2012)

117.

Groome, W.G., Thorkelson, D.J., 2009. The three-dimensional thermo-mechanical signature of ridge subduction and slab window migration. Tectonophysics 464, 70-83.

Gutscher, M.-A., 2002. Andean subduction styles and their effect on thermal structure and interplate coupling. Journal of South American Earth Sciences 15, 3-10.

Gutscher, M.-A., Maury, R., Eissen, J.-P., Bourdon, E., 2000a. Can slab melting be caused by flat subduction? Geology 28, 535-538.

Gutscher, M.A., Spakman, W., Bijwaard, H., Engdahl, E.R., 2000b. Geodynamics of flat subduction: Seismicity and tomographic constraints from the Andean margin. Tectonics 19, 814-833.

Hall, C.E., Gurnis, M., Sdrolias, M., Lavier, L.L., Müller, R.D., 2003. Catastrophic initiation of subduction following forced convergence across fracture zones. Earth and Planetary Science Letters 212, 15-30.

Iwamori, H., Richardson, C., Maruyama, S., 2007. Numerical modeling of thermal structure, circulation of H2O, and magmatism–metamorphism in subduction zones: Implications for evolution of arcs. Gondwana Research 11, 109-119.

Jarrard, R.D., 1986. Relations among subduction parameters. Reviews of Geophysics 24, 217-284.

Kay, S.M., Abbruzzi, J.M., 1996. Magmatic evidence for Neogene lithospheric evolution of the central Andean "flat-slab" between 30 degrees S and 32 degrees S. Tectonophysics 259, 15-28.

Kay, S.M., Mpodozis, C., 2001. Central Andean ore deposits linked to evolving shallow subduction systems and thickening crust. GSA today 11, 4-9.

Lallemand, S., Heuret, A., Boutelier, D., 2005. On the relationships between slab dip, back-arc stress, upper plate absolute motion, and crustal nature in subduction zones. Geochemistry, Geophysics, Geosystems 6, Q09006.

Leng, W., Guinis, M., 2015. Subduction initiation at relic arcs. Geophysical Research Letters, 42, 7014-7021.

Lu, G., Kaus, B., Zhao, L., Zheng, T., 2015. Self-consistent subduction initiation induced by mantle flow. Terra Nova, 27, 130-138.

Li Z.H., Gerya T.V., 2009. Polyphase formation and exhumation of high- to ultrahigh-pressure rocks in continental subduction zone: Numerical modeling and application to the Sulu ultrahigh-pressure terrane in eastern China. Journal of Geophysical Research: Solid Earth, 114, B09406.

Li Z.H. 2014. A review on the numerical geodynamic modeling of continental subduction, collision and exhumation. Sci China Earth Sci, 57: 47–69

Li, Z.H., Gerya, T.V., Burg, J.P., 2010. Influence of tectonic overpressure on P-T paths of HP-UHP rocks in continental collision zones: thermomechanical modelling. Journal of Metamorphic Geology 28, 227-247.

Li, Z.H., Xu, Z.Q., Gerya, T.V., 2011. Flat versus steep subduction: Contrasting modes for the formation and exhumation of high- to ultrahigh-pressure rocks in continental collision zones. Earth and Planetary Science Letters 301, 65-77.

Li, Z.H., Ribe, N.M., 2012. Dynamics of free subduction from 3-D boundary element

modeling. Journal of Geophysical Research: Solid Earth, 117, B06408, doi:10.1029/2012JB009165.

Li Z.-H., Di Leo J.F., Ribe N.M., 2014. Subduction-induced mantle flow, finite strain and seismic anisotropy: Numerical modeling. Journal of Geophysical Research: Solid Earth, 119, 5052-5076.

Li, Z.-X., Li, X.-H., 2007. Formation of the 1300-km-wide intracontinental orogen and postorogenic magmatic province in Mesozoic South China: A flat-slab subduction model. Geology 35, 179-182.

Martinod, J., Husson, L., Roperch, P., Guillaume, B., Espurt, N., 2010. Horizontal subduction zones, convergence velocity and the building of the Andes. Earth and Planetary Science Letters 299, 299-309.

Manea, V., Manea, M., Kostoglodov, V., Sewell, G., 2006. Intraslab seismicity and thermal stress in the subducted Cocos plate beneath central Mexico. Tectonophysics 420, 389-408.

Manea, V., Gurnis, M., 2007. Subduction zone evolution and low viscosity wedges and channels. Earth and Planetary Science Letters 264, 22.

Manea, V.C., Pérez-Gussinyé, M., Manea, M., 2012. Chilean flat slab subduction controlled by overriding plate thickness and trench rollback. Geology 40, 35-38.

Marques, F.O., Nikolaeva, K., Assumpção, M., Gerya, T.V., Bezerra, F.H.R., do Nascimento, A.F., Ferreira, J.M., 2013. Testing the influence of far-field topographic forcing on subduction initiation at a passive margin. Tectonophysics 608, 517-524.

McKenzie, D.P., 1969. Speculations on the consequences and causes of plate motions. Geophysical Journal International 18, 1-32.

McKenzie, D., Jackson, J., Priestley, K., 2005. Thermal structure of oceanic and continental lithosphere. Earth and Planetary Science Letters 233, 337-349.

Morgan, J.P., Hasenclever, J., Shi, C., 2013. New observational and experimental evidence for a plume-fed asthenosphere boundary layer in mantle convection. Earth and Planetary Science Letters 366, 99-111.

Morris, P.A., 1995. Slab Melting as an Explanation of Quaternary Volcanism and Aseismicity in Southwest Japan. Geology 23, 395-398.

Nikolaeva, K., Gerya, T., Marques, F., 2010. Subduction initiation at passive margins: numerical modeling. Journal of Geophysical Research: Solid Earth (1978–2012) 115.

Parsons, B., Sclater, J.G., 1977. An analysis of the variation of ocean floor bathymetry and heat flow with age. Journal of Geophysical Research 82, 803-827.

Perez-Gussinye, M., Lowry, A.R., Morgan, J.P., Tassara, A., 2008. Effective elastic thickness variations along the Andean margin and their relationship to subduction geometry. Geochemistry Geophysics Geosystems 9.

Petford, N., Atherton, M., 1996. Na-rich partial melts from newly underplated basaltic crust: The Cordillera Blanca Batholith, Peru. Journal of petrology 37, 1491-1521.

Pilger, R.H., 1981. Plate Reconstructions, Aseismic Ridges, and Low-Angle Subduction beneath the Andes. Geological Society of America Bulletin 92, 448-456.

Replumaz, A., Capitanio, F.A., Guillot, S., Negredo, A.M., Villaseñor, A., 2014. The coupling of Indian subduction and Asian continental tectonics. Gondwana Research 26, 608-626.

Ribe, N. M. (2010), Bending mechanics and mode selection in free subduction: A thin-sheet analysis, Geophys. J. Int., 180, 559 – 576.

Ricard, Y., Doglioni, C., Sabadini, R., 1991. Differential Rotation between Lithosphere and Mantle - a Consequence of Lateral Mantle Viscosity Variations. Journal of Geophysical Research-Solid Earth and Planets 96, 8407-8415.

Rodriguez-Gonzalez, J., Negredo, A.M., 2012. The role of the overriding plate thermal state on slab dip variability and on the occurrence of flat subduction. Geochemistry Geophysics Geosystems 13.

Sak, P.B., Fisher, D.M., Gardner, T.W., Marshall, J.S., LaFemina, P.C., 2009. Rough crust subduction, forearc kinematics, and Quaternary uplift rates, Costa Rican segment of the Middle American Trench. Geological Society of America Bulletin 121, 992-1012.

Shahraki, M., Schmeling, H., 2012. Plume-induced geoid anomalies from 2D axi-symmetric temperature- and pressure-dependent mantle convection models. Journal of Geodynamics 59–60, 193-206.

Sigloch, K., McQuarrie, N., Nolet, G., 2008. Two-stage subduction history under North America inferred from multiple-frequency tomography. Nature Geoscience 1, 458-462.

Sizova, E., Gerya, T., Brown, M., 2014. Contrasting styles of Phanerozoic and

Precambrian continental collision. Gondwana Research 25, 522-545.

Skinner, S.M., Clayton, R.W., 2011. An Evaluation of Proposed Mechanisms of Slab Flattening in Central Mexico. pure and applied geophysics 168, 1461-1474.

Snyder, W.S., Dickinson, W.R., Silberman, M.L., 1976. Tectonic Implications of Space-Time Patterns of Cenozoic Magmatism in Western United-States. Earth and Planetary Science Letters 32, 91-106.

Sobolev, S.V., Babeyko, A.Y., 2005. What drives orogeny in the Andes? Geology 33, 617-620.

Stevenson, D.J., Turner, J.S., 1977. Angle of Subduction. Nature 270, 334-336.

Suarez, G., Monfret, T., Wittlinger, G., David, C., 1990. Geometry of Subduction and Depth of the Seismogenic Zone in the Guerrero Gap, Mexico. Nature 345, 336-338.

Thielmann, M., Kaus, B.J.P., 2012. Shear heating induced lithospheric-scale localization: Does it result in subduction? Earth and Planetary Science Letters 359–360, 1-13.

Toussaint, G., Burov, E., Avouac, J.P., 2004. Tectonic evolution of a continental collision zone: A thermomechanical numerical model. Tectonics 23, TC6003.

Tovish, A., Schubert, G., Luyendyk, B.P., 1978. Mantle Flow Pressure and the Angle of Subduction - Non-Newtonian Corner Flows. Journal of Geophysical Research 83, 5892-5898.

Turcotte, D.L., Schubert, G., 2002. Geodynamics. Cambridge University Press.

Ueda, K., Gerya, T., Sobolev, S.V., 2008. Subduction initiation by thermal–chemical

plumes: numerical studies. Physics of the Earth and Planetary Interiors 171, 296-312.

Uyeda, S., Kanamori, H., 1979. Back-Arc Opening and the Mode of Subduction. Journal of Geophysical Research 84, 1049-1061.

van Dinther, Y., Morra, G., Funiciello, F., Faccenna, C., 2010. Role of the overriding plate in the subduction process: Insights from numerical models. Tectonophysics 484, 74-86.

van Hunen, J., van den Berg, A.P., 2008. Plate tectonics on the early Earth: limitations imposed by strength and buoyancy of subducted lithosphere. Lithos 103, 217-235.

van Hunen, J., van den Berg, A.P., Vlaar, N.J., 2000. A thermo-mechanical model of horizontal subduction below an overriding plate. Earth and Planetary Science Letters 182, 157-169.

van Hunen, J., van den Berg, A.P., Vlaar, N.J., 2001. Latent heat effects of the major mantle phase transitions on low-angle subduction. Earth and Planetary Science Letters 190, 125-135.

van Hunen, J., van den Berg, A.P., Vlaar, N.J., 2002a. The impact of the South-American plate motion and the Nazca Ridge subduction on the flat subduction below South Peru. Geophysical Research Letters 29, 35-31-35-34.

van Hunen, J., Van Den BERG, A.P., Vlaar, N.J., 2002b. On the role of subducting oceanic plateaus in the development of shallow flat subduction. Tectonophysics 352, 317-333.

van Hunen, J., van den Berg, A.P., Vlaar, N.J., 2004. Various mechanisms to induce present-day shallow flat subduction and implications for the younger Earth: a numerical parameter study. Physics of the Earth and Planetary Interiors 146, 179-194.

van Keken, P.E., Currie, C., King, S.D., Behn, M.D., Cagnioncle, A., He, J., Katz, R.F., Lin, S.-C., Parmentier, E.M., Spiegelman, M., 2008. A community benchmark for subduction zone modeling. Physics of the Earth and Planetary Interiors 171, 187-197.

Vlaar, N.J., 1983. Thermal Anomalies and Magmatism Due to Lithospheric Doubling and Shifting. Earth and Planetary Science Letters 65, 322-330.

Vogt, K., Gerya, T.V., 2014. From oceanic plateaus to allochthonous terranes: Numerical modelling. Gondwana Research 25, 494-508.

Whattam, S.A., Stern, R.J., 2015. Late Cretaceous plume-induced subduction initiation along the southern margin of the Caribbean and NW South America: The first documented example with implications for the onset of plate tectonics. Gondwana Research 27, 38-63.

Yamato, P., Agard, P., Burov, E., Le Pourhiet, L., Jolivet, L., Tiberi, C., 2007. Burial and exhumation in a subduction wedge: Mutual constraints from thermomechanical modeling and natural P-T-t data (Schistes Lustrés, western Alps). Journal of Geophysical Research 112.

Yamato, P., Burov, E., Agard, P., Le Pourhiet, L., Jolivet, L., 2008. HP-UHP exhumation during slow continental subduction: Self-consistent

thermodynamically and thermomechanically coupled model with application to the Western Alps. Earth and Planetary Science Letters 271, 63-74.

Yoshida, M., 2012. Plume's buoyancy and heat fluxes from the deep mantle estimated by an instantaneous mantle flow simulation based on the S40RTS global seismic tomography model. Physics of the Earth and Planetary Interiors 210–211, 63-74.

Yoshida, M., Ogawa, M., 2005. Plume heat flow in a numerical model of mantle convection with moving plates. Earth and Planetary Science Letters 239, 276-285.

Figure captions

Fig. 1. Map of Pacific seafloor showing the dip of shallow portion (< 125 km depth) of subducting slab (modified from Lallemand et al., 2005; Skinner and Clayton, 2011) and spreading ridges that are associated with flat subduction zones (white crosshatched pattern). The inserted table shows the chief geodynamic settings of the preset-day flat subduction (Gutscher et al., 2000a; Gutscher et al., 2000b; Lallemand et al., 2005).

[a] Cumulative length=5000 km, which represents around 10% of all subduction zone.

[b] α_s is defined as the mean shallow dip between 0 and 125 km; α_d the mean deep dip from depths greater than 125 km.

[c] This age refers to the age of subducting oceanic lithosphere around the trench before sinking into the subduction zone.

[d] v_{cmpn}, v_{subn}, and v_{upn} are the normal component of the velocities: v_{cmp}, v_{sub}, and v_{up} refer to the relative convergence velocity, the absolute velocity of the subducting plate and the absolute velocity of the overriding continental plate, respectively. The positive value means trenchward motion.

Fig. 2. Initial model configuration and boundary conditions. (a) Enlargement (1500×670 km) of the numerical box (4000×670 km). Boundary conditions are indicated in yellow. (b) The zoomed domain of the subduction zone. White lines are isotherms shown for increments 200 °C starting from 100 °C. Colors indicate materials that constitute the different layers within the models. Detailed properties of different rock

types that form the material layers are shown in Supplementary Dataset Tables 2-3. Partially molten rocks are not shown in Fig. 2, but appear at subsequent modeling running (e.g., Figs. 3-8). In the numerical models, the medium-scale layering usually shares the same physical properties, with different colors used only for visualizing slab deformation and structural development.

Fig. 3. Numerical modelling results with variable slab ages (M1-7, M1-8, M1-9, M1-10, M1-11 and M1-12). From (a) to (f), the slab age increase from 10 Ma-old to 60 Ma-old. Other parameters are identical in the experiments and are described in Table 1. All the simulations stop at around 25 Ma. White numbered lines are isotherms in °C.

Fig. 4. Numerical modelling results with variable oceanic crustal thickness (T_{OC}) (M2-6 and M2-7). From (a) to (b), the oceanic crustal thickness increases from 26 km to 29 km. Other parameters are identical in the experiments and are described in Table 1. Both the simulations stop at around 25 Ma. White numbered lines are isotherms in °C.

Fig. 5. Numerical modelling results with variable dip angles of the initial weak zone (M1-16, M1-10 and M1-4). The initial weak zone directly reflects the shape of passive continental margin before initial subduction. From (a) to (c), the initial dip angle decreases from 30° to 20°, then to 15°. Other parameters are identical in the experiments, and are described in Table 1. All the simulations stop at around 25 Ma.

White numbered lines are isotherms in °C.

Fig. 6. Initial viscosity field of models M1-10 and M4-1, in which thicknesses of the overriding continental lithosphere are 120 km and 130 km, respectively. Insert shows the composition fields of the same domain at ~25 Ma with white numbered isothermal lines in °C.

Fig. 7. Numerical modelling results of model M3-6 with absolute subduction velocity of 5 cm/a and absolute trenchward velocity of overriding plate of 5 cm/a at time of (a) 6.4 Ma, (b) 9.5 Ma, (c) 11.2 Ma, and (d) 13.7 Ma. The results show the transformation from normal into flat subduction. Also shown (a`)-(d`) the corresponding effective viscosity field with the calculated velocity. White numbered lines are isotherms in °C.

Fig. 8. Numerical modelling results with variable rheological properties. (a-c) Effective viscosity field for models M5-1, M5-2, and M1-9 at time of 25 Ma, in which relative strengths of the overriding continental crust are timed by 0.1, 0.5 and 1 respectively. Inserts show the corresponding composition fields of the same domain at the same time. (d-f) Initial viscosity field of models M1-10, M6-1, and M6-2, in which relative strength of the subjacent asthenosphere are timed by 1.0, 0.1 and 0.01 respectively. Inserts show the composition fields of the same domain at around 25 Ma.

Fig. 9. Subduction regime diagrams for three different parameters pairs. The asterisks

mark the threshold values indicating the transformation from flat to steep subduction. (a) Dependence of subduction mode on the slab age and the oceanic crustal thickness. Main parameters include an initial subduction angle of 20°, an absolute subduction velocity of 5 cm/a, and 120-km-thick overriding continental lithosphere. (b) Dependence of subduction mode on the initial subduction angle and overriding continental lithospheric thickness. Main parameters include 30 Ma-old oceanic lithosphere with 8 km-thick oceanic crust and an absolute subduction velocity of 5 cm/a. (c) Dependence of subduction mode on the initial subduction angle and overriding continental lithospheric thickness with 60 Ma-old oceanic slab. Other parameters are identical to that in (b). (d) Dependence of subduction mode on the overriding continental absolute trenchward velocity and slab absolute subduction velocity. Main parameters include 40 Ma-old oceanic lithosphere with 8 km-thick oceanic crust, an initial subduction angle of 20°, and 120 km-thick overriding continental lithosphere.

Fig. 10. Schematic representation for the induced mantle flow and pressures on the slab surfaces in the subduction zone with (a) a low absolute trenchward velocity or (b) a high absolute trenchward velocity of the overriding plate. Black arrow (I) and (II) refer to the motion direction of the overriding plate and the subducting slab, respectively. Black arrow (III) means the induced landward mantle flow dominated by the trenchward motion of the overriding plate; black arrow (VI) and (V) represent the integrated mantle flow surrounding the slab resulting from the slab subduction and the

trenchward motion of the overriding plate. The red arrows indicate direction of the pressures exerted on the slab surface, and their length roughly represents the relative magnitude. Under the condition of a high absolute trenchward velocity of the overriding plate, the subducting slab is inclined to be upward bended with decreasing the slab dip angle, mainly attributed to an increase in the suction torque by the combined effects of pressure changes of (1) and (2).

Table 1 Main parameters and numerical modelling results

Model	Initial subduction angle (°)	Slab age (Ma)	T_{OC}[a] (km)	v_{sub}[b] (cm/yr)	v_{up}[b] (cm/yr)	D_{TCL}[c] (km)	RS_{asth}[d]	RS_{CC}[d]	Subduction mode
M1-1	15	10	8	5.0	0	120	1	10	Flat(~800)
M1-2	15	20	8	5.0	0	120	1	10	Flat(~800)
M1-3	15	30	8	5.0	0	120	1	10	Flat(~600)
M1-4	15	40	8	5.0	0	120	1	1	Flat(~650)
M1-5	15	50	8	5.0	0	120	1	1	Flat(~900)
M1-6	15	60	8	5.0	0	120	1	1	Flat(~800)
M1-7	20	10	8	5.0	0	120	1	1	Flat(~750)
M1-8	20	20	8	5.0	0	120	1	1	Flat(700)
M1-9	20	30	8	5.0	0	120	1	1	Flat(~850)
M1-10	20	40	8	5.0	0	120	1	1	Steep
M1-11	20	50	8	5.0	0	120	1	1	Steep
M1-12	20	60	8	5.0	0	120	1	1	Steep
M1-13	30	10	8	5.0	0	120	1	1	Flat(~800)
M1-14	30	20	8	5.0	0	120	1	1	Steep
M1-15	30	30	8	5.0	0	120	1	1	steep
M1-16	30	40	8	5.0	0	120	1	1	steep
M2-1	20	40	11	5.0	0	120	1	1	Flat(~800)
M2-2	20	50	14	5.0	0	120	1	1	Steep
M2-3	20	50	17	5.0	0	120	1	1	Flat(~900)
M2-4	20	60	17	5.0	0	120	1	1	Steep
M2-5	20	60	20	5.0	0	120	1	1	Flat(~850)
M2-6	20	80	26	5.0	0	120	1	1	Steep
M2-7	20	80	29	5.0	0	120	1	1	Flat(~800)
M2-8	30	30	14	5.0	0	120	1	1	Steep
M2-9	30	30	17	5.0	0	120	1	1	Flat(~800)
M2-10	30	40	17	5.0	0	120	1	1	Steep
M2-11	30	40	20	5.0	0	120	1	1	Flat(~800)
M3-1	20	40	8	1.0	0	120	1	1	Steep
M3-2	20	40	8	1.0	1.0	120	1	1	Flat(~600)
M3-3	20	40	8	2.5	0	120	1	1	Steep
M3-4	20	40	8	2.5	1.0	120	1	1	Flat(~650)
M3-5	20	40	8	5.0	4.0	120	1	1	Steep
M3-6	20	40	8	5.0	5.0	120	1	1	Flat(~800)
M4-1	20	40	8	5.0	0	130	1	1	Flat(~850)
M4-2	20	40	8	5.0	0	140	1	1	Flat(~850)
M5-1	20	30	8	5.0	0	120	1	0.1	Steep
M5-2	20	30	8	5.0	0	120	1	0.5	Flat(~750)
M6-1	20	40	8	5.0	0	120	0.1	1	Steep
M6-2	20	40	8	5.0	0	120	0.01	1	Flat(~850)

a T_{OC} is the oceanic crustal thickness.

b v_{sub} and v_{up} are absolute velocities of the subducting oceanic slab and overriding continental lithosphere, with positive values indicating trenchward direction.

c D_{TCL} is the thickness of thermal overriding continental lithosphere, with the 1300 °C thermal boundary temperature at the bottom of the TCL.

d RS_{asth} and RS_{CC} are relative strength of asthenosphere and continental crust, respectively, which times the reference A_D in Supplementary Dataset Table 2. For the models M1-1~M1-3, strong overriding continental crust is intentionally set to keep the subduction continuing steadily.

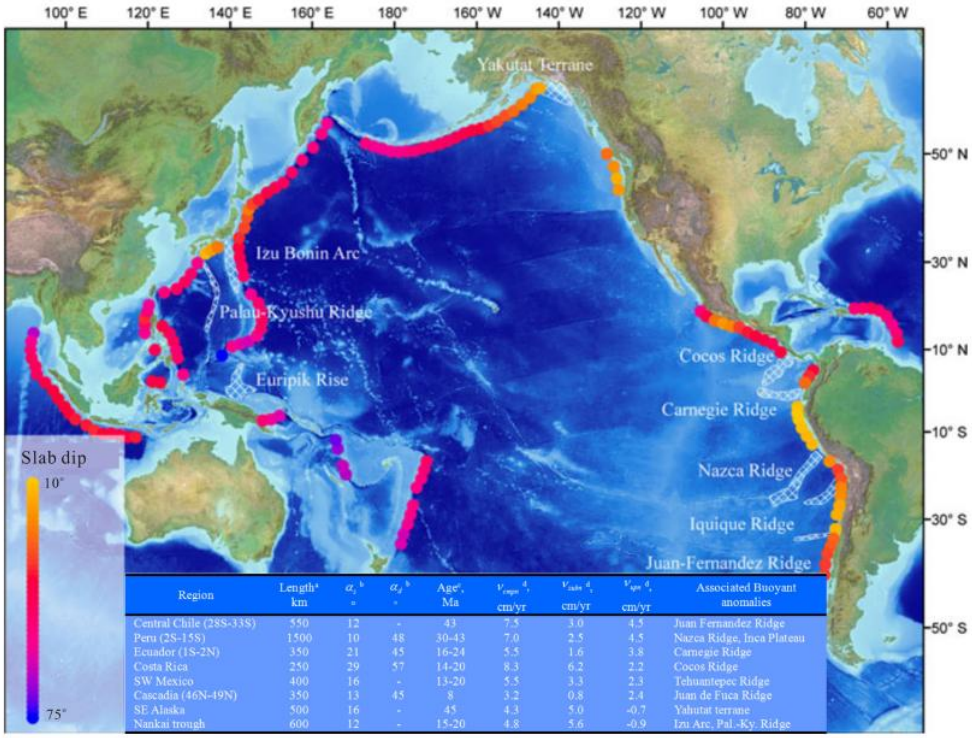

Region	Length[a] km	α_1 [b] °	α_2 [b] °	Age[c], Ma	v_{conv} [d], cm/yr	v_{subd} [d], cm/yr	v_{sp} [d], cm/yr	Associated Buoyant anomalies
Central Chile (28S-33S)	550	12	-	43	7.5	3.0	4.5	Juan Fernandez Ridge
Peru (2S-15S)	1500	10	48	30-43	7.0	2.5	4.5	Nazca Ridge, Inca Plateau
Ecuador (1S-2N)	350	21	45	16-24	5.5	1.6	3.8	Carnegie Ridge
Costa Rica	250	29	57	14-20	8.3	6.2	2.2	Cocos Ridge
SW Mexico	400	16	-	13-20	5.5	3.3	2.3	Tehuantepec Ridge
Cascadia (46N-49N)	350	13	45	8	3.2	0.8	2.4	Juan de Fuca Ridge
SE Alaska	500	16	-	45	4.3	5.0	-0.7	Yalutat terrane
Nankai trough	600	12	-	15-20	4.8	5.6	-0.9	Izu Arc, Pal.-Ky. Ridge

Fig. 1. Pengpeng Huangfu and coauthors

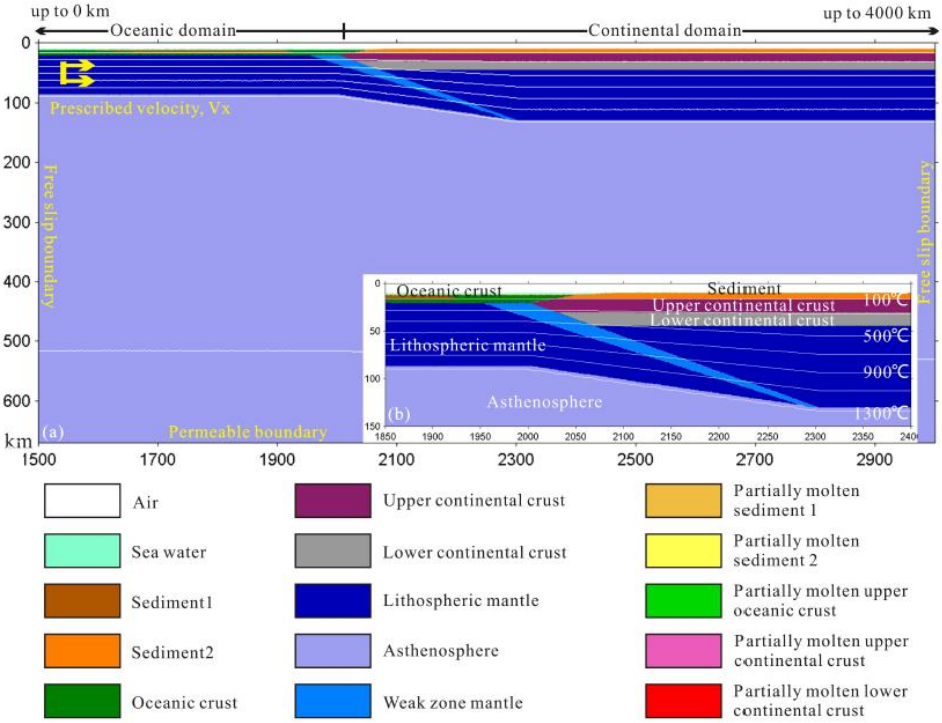

Fig. 2. Pengpeng Huangfu and coauthors

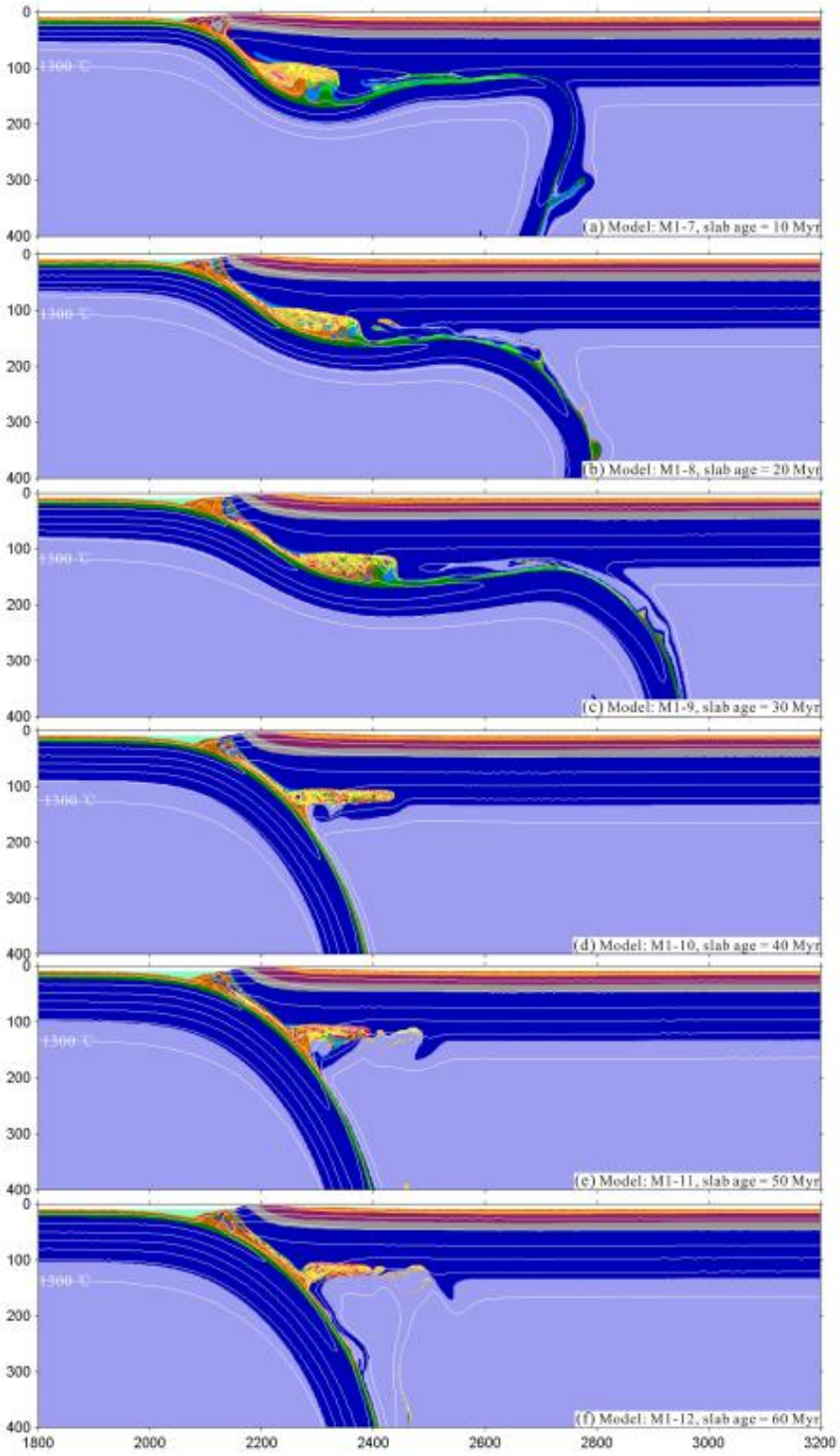

Fig. 3. Pengpeng Huangfu and coauthors

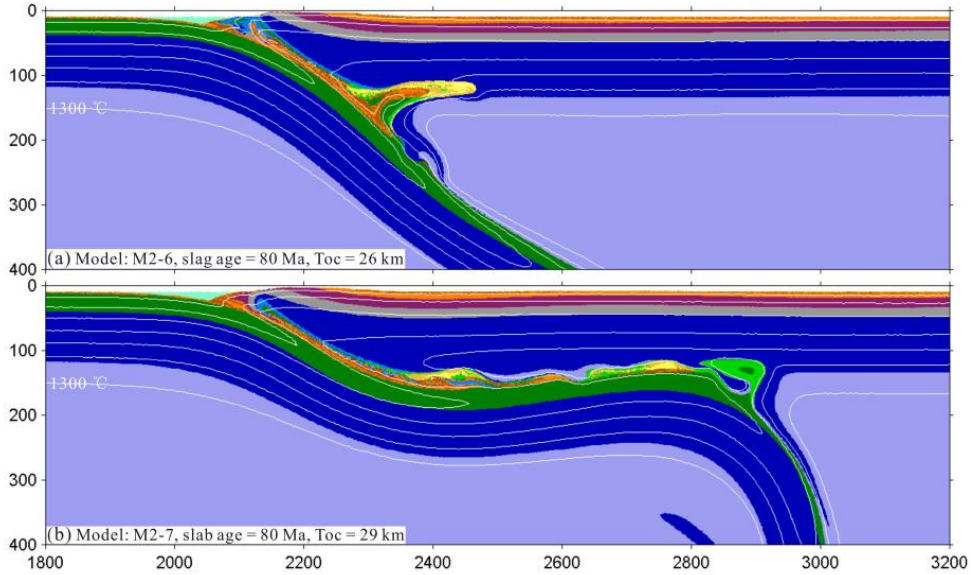

Fig. 4. Pengpeng Huangfu and coauthors

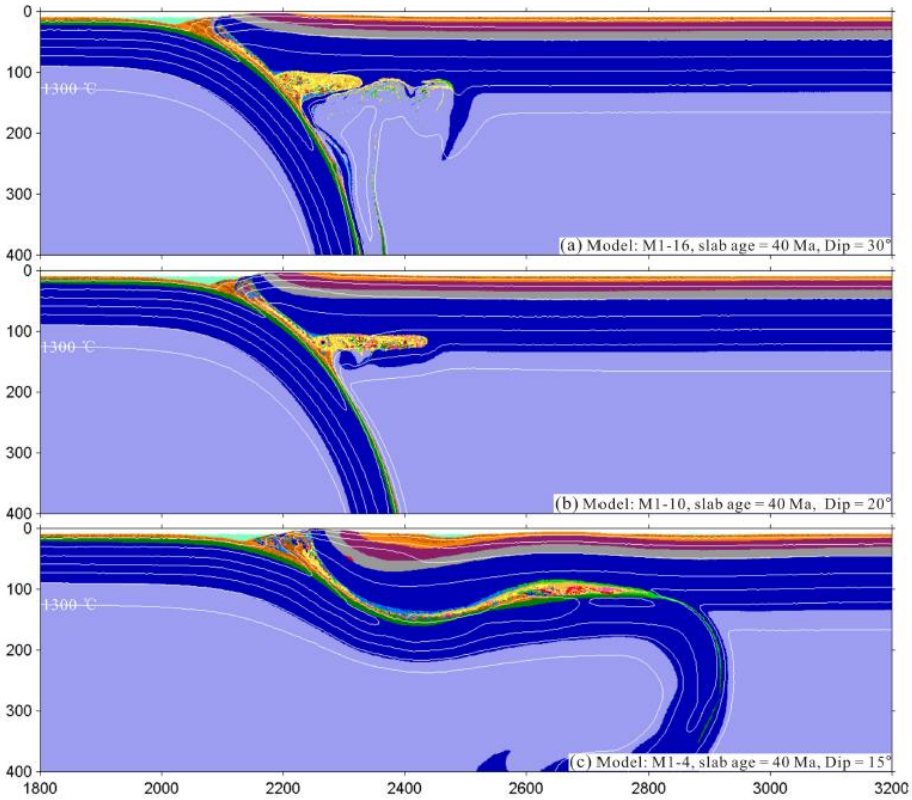

Fig. 5. Pengpeng Huangfu and coauthors

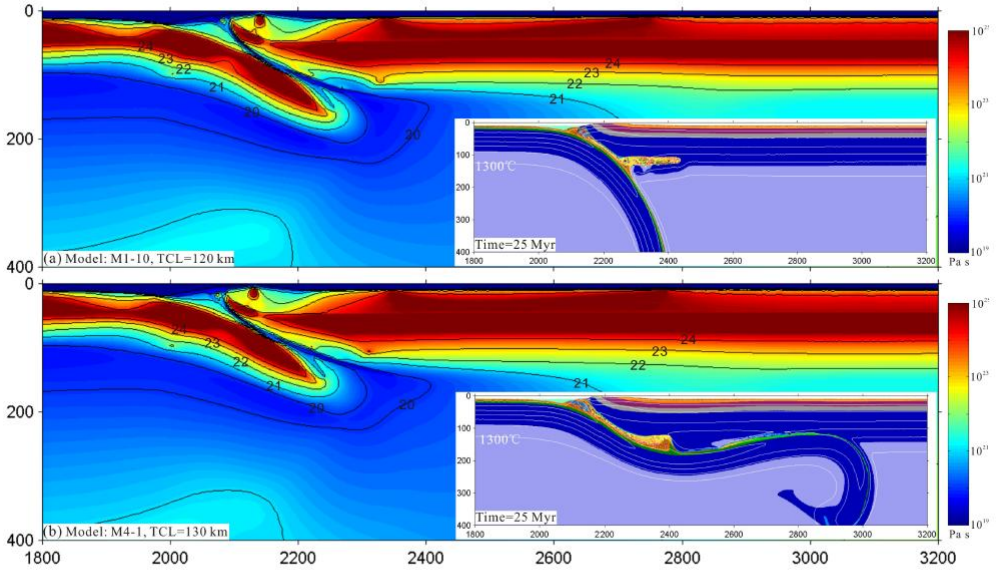

Fig. 6. Pengpeng Huangfu and coauthors

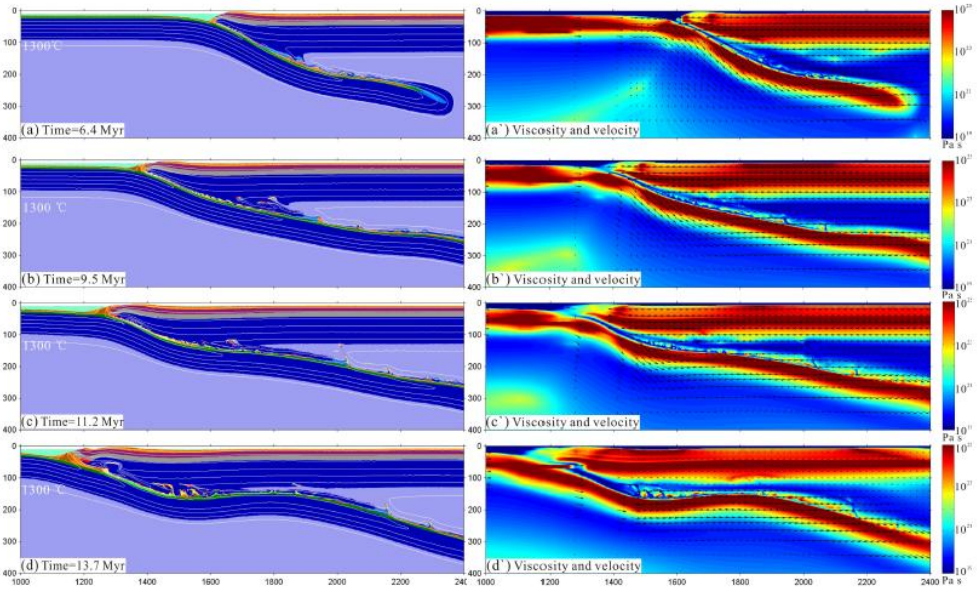

Fig. 7. Pengpeng Huangfu and coauthors

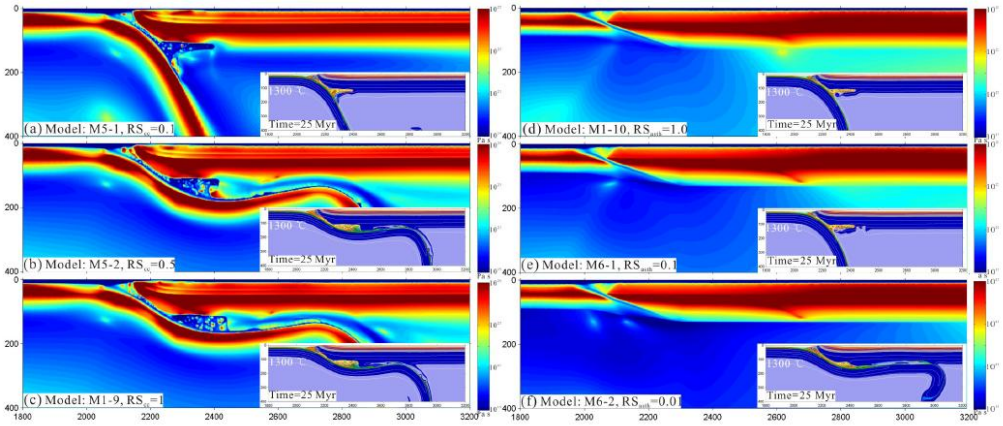

Fig. 8. Pengpeng Huangfu and coauthors

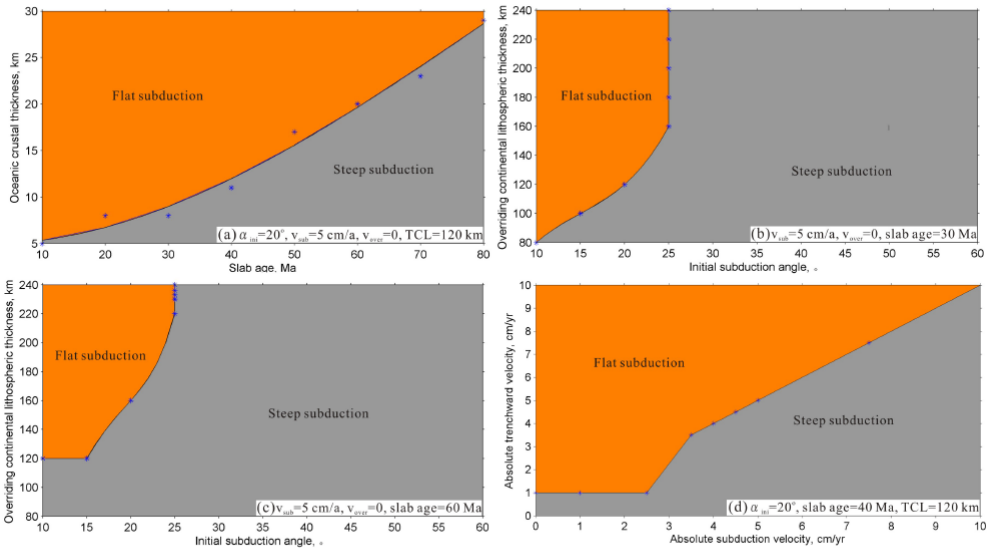

Fig. 9. Pengpeng Huangfu and coauthors

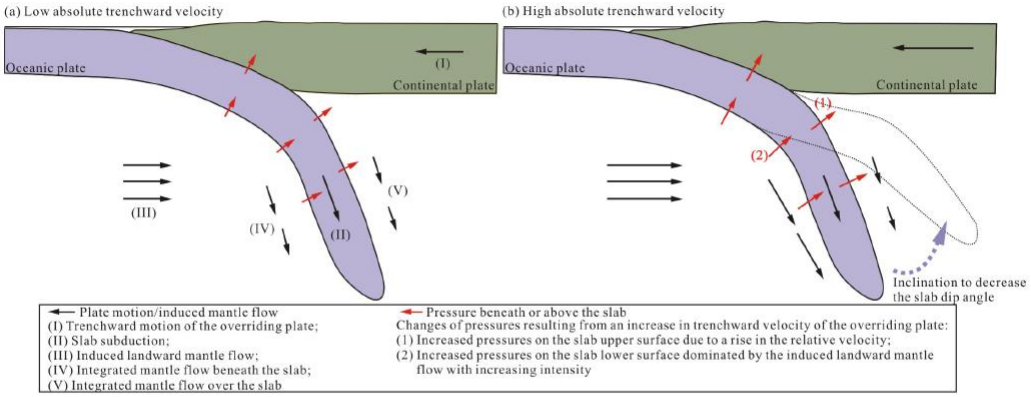

Fig. 10. Pengpeng Huangfu and coauthors

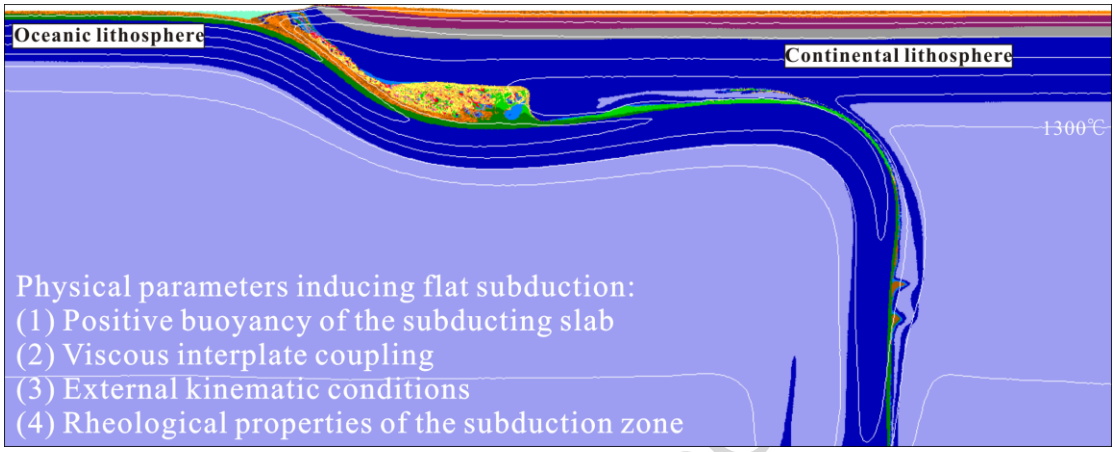

Graphical abstract

Highlights:

- Physical parameters that control flat subduction are classified into four categories.
- Positive buoyancy is the primary control on the formation of flat subduction.
- Interplate coupling and external kinematic conditions also influence Flat subduction.
- Slab dip variability has a first-order dependence on gravitational torque and suction torque.